Nanoscale Advances

REVIEW

View Article Online
View Journal | View Issue

Cite this: *Nanoscale Adv.*, 2020, **2**, 4341

Rare-earth-free magnetically hard ferrous materials

Zefan Shao[a] and Shenqiang Ren *[abc]

Permanent magnets, especially rare-earth based magnets, are widely used in energy-critical technologies in many modern applications, involving energy conversion and information technologies. However, the environmental impact and strategic supplies of rare-earth elements hamper the long-term development of permanent magnets. Hence, there is a surge of interest to expand the search for rare-earth-free magnets with a large energy product $(BH)_{max}$. Among these rare-earth-free magnets, iron-based permanent magnets emerge as some of the most promising candidates due to their abundance and magnetic performance. In this review, we present a summary of iron-based permanent magnets from materials synthesis to their magnetic properties.

Received 24th June 2020
Accepted 25th July 2020

DOI: 10.1039/d0na00519c

rsc.li/nanoscale-advances

1 Introduction

Permanent magnets have received intense interest due to their applications in energy-critical technologies, such as wind turbine, electric vehicles and information storage.[1–8] The essential measure of permanent magnets is the energy product,[9,10] which is defined as the product of B and H in the second quadrant hysteresis curve.[11,12] Rare-earth magnets include neodymium magnets and samarium–cobalt magnets.[13–15] However, considering the rapidly increasing demand for rare-earth elements in various areas (Fig. 1a), much attention has been focused on searching for new alternative magnets with rare-earth-free elements.[16,17] The rare-earth-free magnetic materials with high magneto-crystalline anisotropy and energy product exhibit promising potential for use as permanent magnets (Fig. 1b and Table 1).[16,18]

Among many pursued rare-earth-free elements, iron has been emerging as one of the most promising candidates due to

[a]*Department of Mechanical and Aerospace Engineering, University at Buffalo, The State University of New York, Buffalo, NY 14260, USA*
[b]*Department of Chemistry, University at Buffalo, The State University of New York, Buffalo, NY 14260, USA*
[c]*Research and Education in Energy, Environment & Water (RENEW) Institute, University at Buffalo, The State University of New York, Buffalo, NY 14260, USA. E-mail: shenren@buffalo.edu*

Mr. Zefan Shao is a graduate student of Mechanical and Aerospace Engineering at the University at Buffalo, The State University of New York. He joined the laboratory of Prof. Shenqiang Ren, working on solution-based synthesis of colloidal functional nanomaterials. His research interests focus on functional metal and alloy nanoparticles.

Dr. Shenqiang Ren is Professor of Mechanical and Aerospace Engineering, and Chemistry at SUNY-Buffalo, with research interests in emerging functional materials and devices. He earned his PhD degree in Materials Science and Engineering at the University of Maryland College Park, and then served as a postdoctoral fellow at the Massachusetts Institute of Technology (MIT). He received the 2015 National Science Foundation – CAREER Award, 2014 Army Research Office – Young Investigator Award, 2013 NSF EPSCOR First Award, 2013 Air Force Summer Faculty Fellowship, 2009 Dean's Doctoral Research Award and Distinguished Doctoral Dissertation Award at the University of Maryland, College Park.

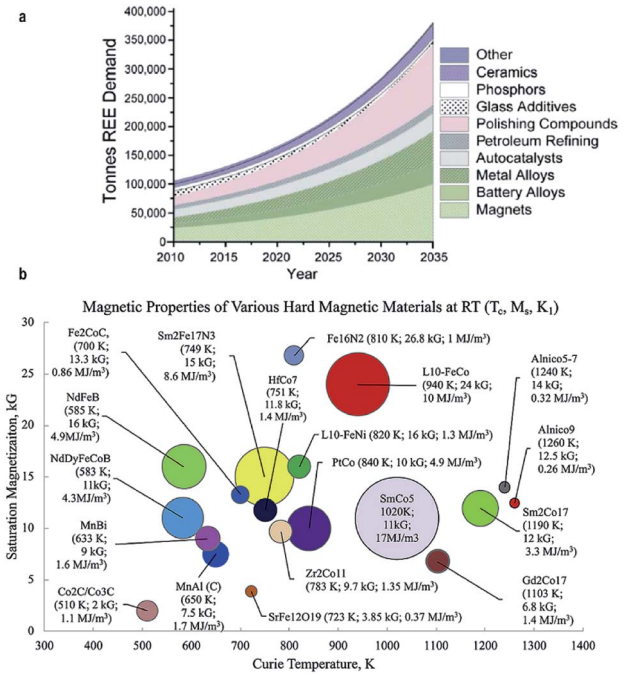

Fig. 1 (a) Evolution of market distribution of REE demand; (b) magnetic properties of various hard magnetic materials. Reproduced from ref. 16,17 and 18 with the permission of Elsevier, American Chemical Society and Springer Nature.

Table 1 Magnetic properties of rare-earth-free magnets

Hard magnet	Magnetocrystalline anisotropy, MJ m^{-3}	Saturation magnetization, kG
$Fe_{16}N_2$	2.0	28.3 (ref. 36 and 37)
$L1_0FeCo$	0.1	24.5 (ref. 38)
$L1_0FePt$	6.6	13.8 (ref. 39 and 40)
$L1_0FeNi$	1.3	14.7 (ref. 41)
$L1_0FePd$	1.8	13.7 (ref. 40 and 42)
Zr_2Co_{11}	1.1	7.8 (ref. 43 and 44)
MnBi	1.0	8.2 (ref. 45 and 46)
MnAl	1.8	7.5 (ref. 47 and 48)
Alnico 9	0.2	11.2 (ref. 49 and 50)
Alnico 5–7	0.1	13.5 (ref. 50 and 51)

its abundance and large saturation magnetization.[19,20] The ferrites have shown their applications in navigation from ancient times.[11,21] Iron-based magnets with a large coercivity, such as FePd, FePt, FeCo, $Fe_{12}N_2$, ε-Fe_2O_3, FeNi and Fe_3Se_4, would present great potential for green energy applications due to their high saturation magnetization and magnetocrystalline anisotropy. In this context, the tetragonal $L1_0$-ordered phase of FePd and FePt can achieve an optimum coercivity of 16 kOe, whereas the FeCo alloy has shown a higher value of uniaxial magnetocrystalline anisotropy (K_u) of 1×10^7 J.[22,23] Meanwhile, the magnetic energy product for the $Fe_{16}N_2$ phase can reach 20 MGOe.[19,24] In the past several decades, much attention and efforts have been focused on investigating the manufacturing routes and magnetic properties of these iron-based materials.[25,26] Hard ferrites, some of the least expensive and most common magnets, are composed of fine particles with a tetragonal crystal structure.[27] These iron-based permanent magnets, combined with Ba or Sr, exhibit a pronounced coercivity but relatively low magnetization, attributed to the coexistence of ferromagnetic and antiferromagnetic coupling.[28] The magnetization of these magnets is temperature-dependent and shows an abrupt transition point due to the phase transformation.[29] Alternatively, high coercivity can also be triggered by the dimension and morphology of ferrite hard magnets within the single domain region.[30] The ferrite magnets could exhibit tuneable coercivity (H_c) due to the varied particle size and stoichiometry.[31] Moreover, magnetic properties can be influenced by the exchange coupling interaction between magnetically hard and soft phases.[32,33] In this review, we summarize the strategies for the synthetic control of magnetic properties in iron-based magnets.[34,35]

2 Preparation and magnetic properties of iron-based ferrous materials

Iron-based ferrous materials are some of the rare-earth-free hard magnets with a large uniaxial magnetocrystalline anisotropy.[52] Iron-based magnets, particularly the tetragonal $L1_0$ ordered phase, show promising applications in information storage and electrical machine systems due to their large magnetic anisotropy and high coercivity.[18,53,54] Therefore, intense attention has been focused on the formation of the $L1_0$-ordered phase in iron-based magnets.[55]

2.1 Iron cobalt hard magnet

The FeCo alloy, an important magnetic material, is very attractive due to its high saturation magnetization (M_s) and Curie temperature (T_c) among transition metal alloys, while its small coercive field and low magnetocrystalline anisotropy indicate its soft nature.[56] However, tetragonal distorted FeCo alloys could turn FeCo alloys into hard magnets with high coercivity.[16] The theoretical calculations achieved by Wu *et al.* in 2008 showed a giant uniaxial magnetocrystalline anisotropy and saturation magnetization in body-centered-tetragonal FeCo alloys (Fig. 2a).[57]

The possibility of achieving high magnetocrystalline anisotropy in FeCo alloys was initially inspired by straining metal films on a templated substrate. In 2006, Winkelmann, *et al.* reported the perpendicular magnetic anisotropy induced by pure Fe and Co films grown on Pd (001), showing that the anisotropy energy can be improved by a tetragonal crystal structure.[58] A suitable range of lattice-parameter ratios, known as *c*/*a* values, can promote the formation of tetragonal FeCo, which were proved to be between 1.18 and 1.31 by Warnicke *et al.* in 2007.[59] The exact prerequisites, obtained using the *c*/*a* ratio, promote the synthesis of a tetragonal crystal structure of an FeCo alloy and provide a potential direction for high magnetocrystalline anisotropy. In 2012, Kim and Hong reported that the energy product of FeCo grown on an FePt (001) substrate, as shown in Fig. 2b, can reach 66 MGOe and the maximum

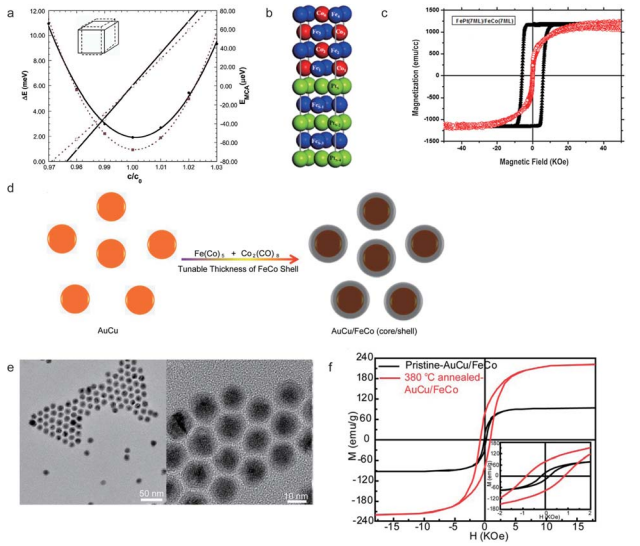

Fig. 2 (a) The calculated total energy (ΔE) and magnetocrystalline anisotropy energy (E_{MCA}) of FeCo along the (001) direction; (b) a schematic illustration of the crystal structure of FeCo/FePt(001); (c) magnetic hysteresis loops for an FeCo/FePt thin film; (d) schematic figure of the AuCu/FeCo (core/shell) nanocrystal synthesis; (e) the TEM image of AuCu/FeCo (core/shell) nanoparticles; (f) the M–H loops of $L1_0$ AuCu/FeCo particles. The inset shows the annealing temperature-dependent coercivity of $L1_0$ AuCu/FeCo. Reproduced from ref. 42, 45, 46 and 48 with the permission of AIP Publishing, Elsevier and American Chemical Society.

coercivity, guided by a full potential linearized augmented plane wave (FLAPW) method, is 188 kOe.[60] In 2015, Giannopoulos introduced an advanced FeCo ultrathin layer grown on an $L1_0$ FePt film, which shows a maximum energy product of up to 50 MGOe and a maximum coercive field of 50 kOe, as shown in Fig. 2c.[61] These discoveries clearly show the potential applications of FeCo alloys in permanent magnets. In 2014, the interstitial boron doped FeCo, introduced by Khan and Hong, indicated that the magnetocrystalline anisotropy constant can reach 0.8 MJ m^{-3} with an estimated energy product of 100 MGOe.[62] The preparation of tetragonal distorted FeCo magnets reported so far has been through similar routes by synthesizing under a high temperature and oxygen-free environment. The average diameter of FeCo particles, synthesized in this method, inevitably increases with the rise of temperature. The magnetic properties, such as coercivity, can be weakened with a large size of FeCo particles. A long-standing challenge of controlling the particle size has been overcome by utilizing an AuCu/FeCo (core/shell) structure (Fig. 2d), introduced by Ren in 2014. This approach presents a tetragonal FeCo microstructure which is induced by the $L1_0$ ordering of the AuCu core, with an average diameter of 10 nm and a significantly high coercivity and magnetization with the values of 846 Oe and 221 emu g^{-1}, as shown in Fig. 2e and f.[63]

2.2 Iron platinum and iron palladium hard magnets

Precious metal ferromagnets, such as FePd and FePt, have shown a large magnetocrystalline anisotropy due to their crystal structure.[64] The $L1_0$ ordered FePd and FePt alloys show a large magnetocrystalline anisotropy.[18] The microstructure of hard magnet FePd is dominated by a face-centered-tetragonal lattice.

2.2.1 Iron palladium. Iron palladium (FePd) alloys, achieving high magnetocrystalline anisotropy and energy density, attract intense interest due to their broad applications ranging from data storage to ferrofluids.[65] The colloidal solution synthesis of hard magnetic FePd particles is one of the most studied ones. The formation of a tetragonal FePd lattice, triggered by high temperature sintering, makes the FePd particles exhibit a hard magnetic performance.[66] The phase transformation, induced by high temperature conditions, cannot always control the size of annealed FePd nanoparticles during the sintering process.[67] The simultaneous chemical reaction introduced by Chen and Nikles in 2002 was operated in a three-neck flask by the reduction of palladium acetylacetonate and thermal decomposition of iron pentacarbonyl, which achieved an optimal coercivity of 685 Oe as shown in Table 2.[68] The ordering parameter S, presented in Table 1, was calculated using unit cell parameters (a, c) obtained by X-ray diffraction quantification. The FePd nanoparticles would reach an average diameter of 11 nm after annealing at 700 °C for 3 hours. The development of this simultaneous reaction was limited by its high energy requirement and a lengthy reaction time. In 2006, Watanabe and Sato *et al.* reported a synthesis route for FePd nanoparticles that can be applied in the recording media and fabricated by an electron-beam evaporation technique. The value of the optimal coercivity can reach 1.2 kOe after annealing at 773 K for 1 h (Fig. 3a).[69,70] Meanwhile, the FePd nanoparticles introduced by Sato *et al.* in 2000 were synthesized by a modified polyol process, showing the thermal treatment effect on magnetic properties.[71] Besides, in 2004 Hou *et al.* reported monodisperse FePd nanoparticles, controlled by the ratio and type of stabilizer, presenting an average diameter of 13.5 nm and an optimal coercivity of 350 Oe, as shown in Fig. 3b.[72] The exchange-coupling also played an important role in controlling the formation of $L1_0$-FePd. In 2013, Yu *et al.* reported a one-pot synthesis of $L1_0$-FePd-Fe (Fig. 3c), which was controlled by a thermodynamically stable mixture, with the lattice fringe spacings of 0.27 nm and 0.20 nm (Fig. 3d), indicating an optimal coercivity of 2.6 kOe and a saturation magnetization of 190 emu g^{-1}, as shown in Fig. 3e.[73] A eutectic reaction, known as liquid phase transformation, is based on a solid-state eutectic composition with low melting point to minimize energy consumption which leads to a low-cost manufacturing process.

Table 2 The order parameter and coercivity of an FePd film at different annealing temperatures. Reproduced from ref. 53 with the permission of AIP Publishing

Temperature (°C)	As-prepared	550	600	700	700
Time (min)	0	30	30	60	180
Condition	Vacuum	Vacuum	Vacuum	Ar–H_2	Ar–H_2
a (ppm)	386	383	381	381	379
c (pm)	386	383	381	381	379
S	0	0	0	0	0
H_c (Oe)	12	685	548	421	297

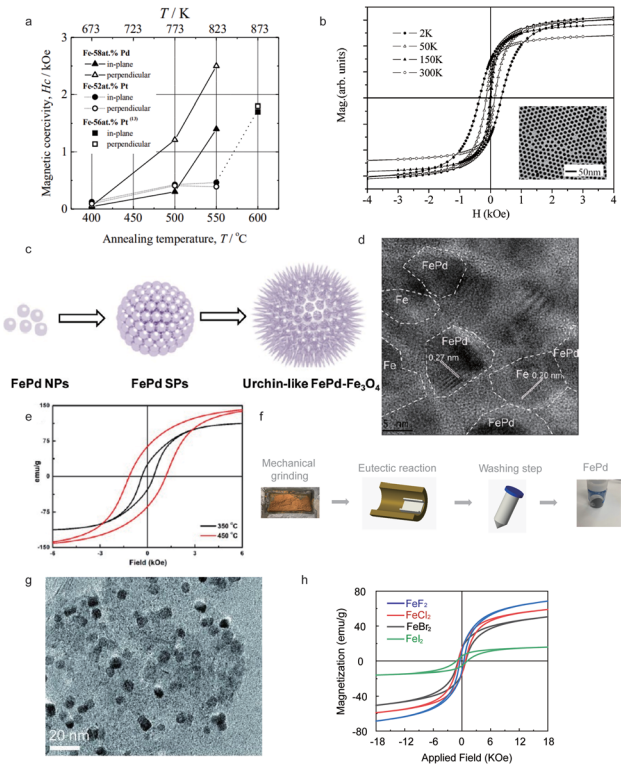

Fig. 3 (a) Annealing temperature dependence of coercivity for FePd nanoparticles dispersed on NaCl (001) substrates covered with a-Al_2O_3 thin films; (b) magnetic hysteresis loops and TEM image of monodisperse FePd; (c) schematic illustration of self-aggregation of FePd–Fe; (d) high-resolution (HRTEM) image of the $L1_0$-FePd-Fe nanoparticles; (e) magnetic hysteresis loops of FePd nanoparticles which are controlled by the exchange-coupling method at different temperatures; (f) eutectic salt melt synthesis and crystallization of FePd powder prepared by a eutectic reaction; (g) the TEM image of FePd nanoparticles prepared by a eutectic reaction; (h) magnetic hysteresis loops of FePd with different precursors prepared by a eutectic reaction. Reproduced from ref. 54, 55, 57, 58 and 59 with the permission of IOP Publishing, Elsevier, American Chemical Society and Royal Society of Chemistry.

Therefore, an understanding of microstructure formation guided by a eutectic reaction is essential for the exploration of advanced magnetic nanoparticle formation. In 2020, Ren introduced a eutectic crystallization approach into the synthesis of FePd nanoparticles with high coercivity.[74]

The schematic eutectic salt melt route, a powder metallurgical method, considers KCl–LiCl as a salt solvent to prepare FePd particles, as shown in Fig. 3f. The TEM image of FePd nanoparticles indicates the average diameter of FePd (50 nm), as shown in Fig. 3g. Fig. 3h illustrates the magnetization–hysteresis (M–H) loops of the as-synthesized FePd nanoparticles, which are prepared using different halide precursors with the same ratio between Fe and Pd. Meanwhile, the optimal precursor for FePd is FeI_2 with a coercivity of 1800 Oe and a magnetization of 17 emu g^{-1}.[74] The eutectic salt melt method can effectively avoid the sintering induced aggregation of magnetic nanoparticles during phase transformation and simplifies the preparation procedure of FePd magnets.

2.2.2 Iron platinum. Iron platinum (FePt), face-centered-cubic (FCC) phase, can be transformed into a face-centered-tetragonal (FCT) phase with a large magnetocrystalline anisotropy after a high temperature thermal annealing.[75] During the past few decades, researchers have developed many synthetic routes to attain FePt with a FCT lattice microstructure, such as one-step thermal synthesis with metal precursors, water-in-oil microemulsion and exchange-coupled assembly. In 1935, $L1_0$ FePt alloys, with a magnetocrystalline anisotropy of 66 Merg cm^{-3}, were synthesized by Graf and Kussmann.[76] The ordered $L1_0$ FePt alloys can be generated by annealing FCC FePt at a certain temperature which is above the FCT ordering temperature. In 2003, Jeyadevan reported a chemical route, achieving the transition of the FCT crystal structure of FePt, with an optimal coercivity of 1.7 kOe at 10 K, as shown in Fig. 4a.[77] Through the decomposition of platinum acetylacetonate and iron pentacarbonyl in the presence of oleic acid and oleylamine, monodisperse FePt was successfully prepared in 2000 by Sun *et al.*[78] In 2003, Sun's group reported fct-FePt (Fig. 4b) nanoparticles obtained from a chemical reaction route, showing a high coercivity of 7.6 kOe (Fig. 4c).[79] The chemical synthesis routes for FePt were the dominating routes in the past few decades. Meanwhile, a long-existing challenge is the aggregation of FePt nanoparticles induced by thermal annealing beyond the single-domain region. In 2004, the synthesis of FePt nanoparticles with tunable size was introduced by Chun *et al.*, where the average diameter of FePt was 6 nm (Fig. 4d and e) and the room temperature coercivity reached 13 kOe.[80] The transformation of the face-centered-tetragonal phase generated from the disordered FCC crystal structure requires a reaction temperature above 650 °C, while the morphology and structure of FePt nanoparticles are likely to be destroyed during the sintering process due to the relatively high temperature. In 2019, Ren *et al.* developed an annealing route known as eutectic melt crystallization of ordered $L1_0$-FePt to synthesize an ordered face-cubic-tetragonal FePt alloy, as shown in Fig. 4f. The as-synthesized $L1_0$-FePt particles exhibited a coercivity of 16 kOe and a saturation magnetization of 33.6 emu g^{-1} with the optimal energy product reaching 5.0 MGOe, as shown in Fig. 4g–i.[81]

2.3 $Fe_{16}N_2$

The $Fe_{16}N_2$ magnet, one of the promising permanent magnet candidates, exhibits a giant saturation magnetization.[82] The synthesis of bulk α''-$Fe_{16}N_2$ was reported (Fig. 5a).[83] In 1972, Kim and Takahashi studied the saturation magnetization and magnetic moment of α''-$Fe_{16}N_2$ which showed a saturation magnetization of 2000 emu cm^{-3}, as shown in Fig. 5b, which is larger than that of FeCo.[84] Due to its high magnetic performance, much attention was paid to the exploration of different types of α''-$Fe_{16}N_2$, such as bulk, nanoparticles and thin films. Subsequently, various synthesis routes were reported, such as the preparation of α''-$Fe_{16}N_2$ nanoparticles using compounds containing Fe_2O_3 and NH_3–H_2 mixed gas, introduced by Bao and Metzger in 1994.[85] These methods mostly produced multiple phases, including α''-$Fe_{16}N_2$, while the magnetic properties can be influenced by the volume ratio of α''-$Fe_{16}N_2$ (Table 3). In 2016, Wang *et al.* reported a route for the synthesis

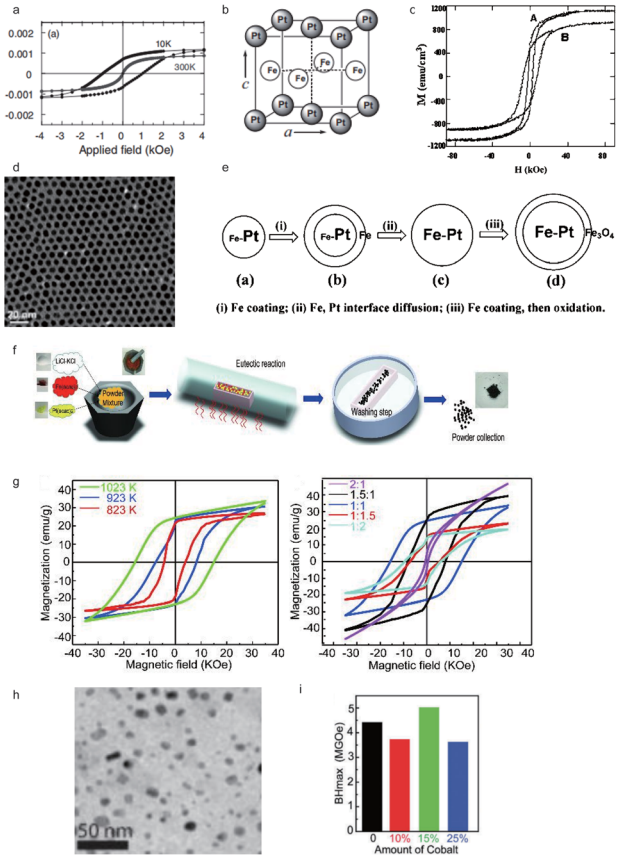

Fig. 4 (a) Magnetic hysteresis loops of FePt prepared by a chemical route at 10 K; (b) schematic illustration of chemically ordered fct-FePt; (c) the TEM image of monodisperse FePt; (d) TEM bright field images of tunable FePt particles; (e) schematic illustration of the FePt nanoparticle formation mechanism; (f) schematic illustration of the synthesis of $L1_0$-FePt; (g) the TEM image of $L1_0$-FePt nanoparticles; (h) magnetic hysteresis loops of $L1_0$-FePt nanoparticles; (i) the calculated energy product of FePt–Co magnets. Reproduced from ref. 62, 64, 65 and 66 with the permission of IOP Publishing, American Chemical Society and Royal Society of Chemistry.

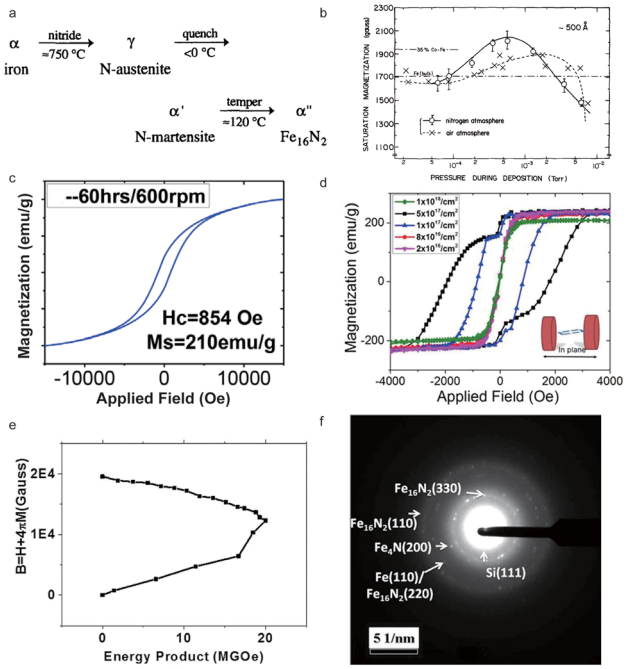

Fig. 5 (a) The formation sequence of $Fe_{16}N_2$; (b) magnetic hysteresis loops of $Fe_{16}N_2$ prepared by ball milling and shock compaction; (c) saturation magnetization of Fe films against pressure which were separately deposited in a nitrogen atmosphere and vacuum; (d) magnetic hysteresis loops of $Fe_{16}N_2$ at room temperature; (e) the calculated energy product for $Fe_{16}N_2$ at room temperature; (f) the TEM diffraction pattern of $Fe_{16}N_2$ with 5×10^{17}ions per cm^2 fluence. Reproduced from ref. 68, 69, 71 and 20 with the permission of Elsevier, AIP Publishing, John Wiley and Sons and Springer Nature.

of $Fe_{16}N_2$ by ball milling and shock compaction, achieving a high saturation magnetization of 210 emu g^{-1} and a large coercivity (H_c) of 854 Oe, as shown in Fig. 5c.[86] Fig. 5d suggests that the coercivity of the synthesized free-standing $Fe_{16}N_2$ foil can reach 1910 Oe. The value of the magnetic energy product of $Fe_{16}N_2$ can reach 20 MGOe at room temperature, proving the potential applications in permanent magnets, as shown in Fig. 5e. Fig. 5f indicates the crystalline structure through the TEM diffraction pattern.[19]

2.4 ε-Fe_2O_3

Iron oxides exist as different crystalline polymorphs, such as α-, β-, γ-, and ε-Fe_2O_3.[87] Among these iron oxides, ε-Fe_2O_3 is of much interest due to its unique magnetic properties.[88] The ε-Fe_2O_3 formed under exclusively high temperature conditions exhibits potential applications in recording media and microwave devices.[89] The silica template methods, depending on the chemical reaction, have been the most common synthesis routes in the past several decades. In 2004, Jin, Ohkoshi and Hashimoto reported nanosized ε-Fe_2O_3, prepared in a silica matrix, which showed a giant coercive field of 20 kOe at room temperature (Fig. 6a).[90] In 2008, Sakurai *et al.* introduced an advanced route to synthesize ε-Fe_2O_3 nanoparticles with an average diameter of 7 nm by combining the reverse-micelle and sol–gel methods (Fig. 6b), as shown in Fig. 6c.[91] In 2012, Namai reported a nanocrystalline ε-Fe_2O_3 (Fig. 6d), prepared by a nanoscale chemical synthesis in a silica template (Fig. 6e), presenting a large coercivity value of 31 kOe (Fig. 6f).[92] The two-step magnetic transition was dependent on temperature and the external magnetic field. In 2015, Kohout *et al.* reported ^{57}Fe isotope enriched ε-Fe_2O_3, prepared by a sol–gel technique in a silica template, which exhibited a coercivity H_C of 21 kOe at 300 K, as shown in Fig. 6g.[93] A significant improvement of

Table 3 Magnetic properties of $Fe_{16}N_2$. Reproduced from ref. 70 with the permission of AIP Publishing

Species	Site	H_{hf}	ΔE_Q	IS
α″-$Fe_{16}N_2$	FeI	292	−0.17	0.01
α″-$Fe_{16}N_2$	FeII	397	−0.04	0.07
α″-$Fe_{16}N_2$	FeIII	317	0.15	0.10
α-Fe	—	330	0	0
γ-Austenite	—	—	—	0.04
	—	—	0.37	0.07

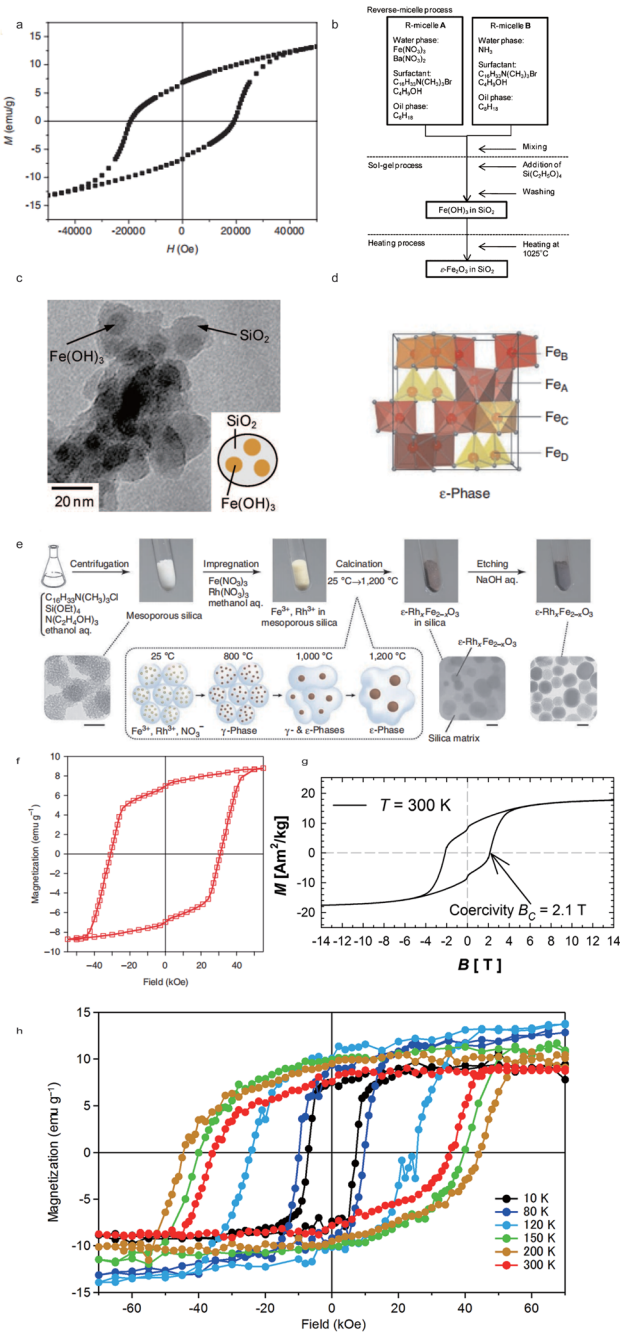

Fig. 6 (a) Magnetic hysteresis loops of ε-Fe_2O_3 prepared by Jin *et al.*; (b) procedure to prepare SiO_2-coated ε-Fe_2O_3 nanorods; (c) TEM image of ε-Fe_2O_3; (d) crystal structure of the ε-phase; (e) schematic illustration of synthesis of ε-Fe_2O_3 on a silica template; (f) magnetic hysteresis loops of oriented ε-Fe_2O_3 at 300 K; (g) magnetic hysteresis loops of powdered ε-Fe_2O_3 embedded in a silica matrix at 300 K; (h) magnetic hysteresis loops of ε-Fe_2O_3 oriented at different temperatures. Reproduced from ref. 75, 76, 77, 78 and 79 with the permission of John Wiley and Sons, Springer Nature, and AIP Publishing.

magnetic properties for ε-Fe_2O_3 was reported by Ohkoshi *et al.* in 2017.[94] The attained ε-Fe_2O_3, prepared using metal instead of traditional iron ions, showed the highest coercivity of 45 kOe at 200 K, as shown in Fig. 6h.

2.5 FeNi

The $L1_0$-FeNi phase, known as tetrataenite ($Fe_{50}Ni_{50}$), is one of the rare-earth-free magnet candidates.[95] In 1962, Pauleve *et al.* reported $L1_0$-FeNi induced by neutron irradiation and annealed at 593 K under a magnetic field.[96] The order–disorder transition temperature of $L1_0$-FeNi is shown to be 593 K, further proved by Reuter *et al.* in 1989 under electron irradiation.[97] As the atomic jump of nickel in FeNi alloys could take more than 10 000 years at 573 K,[98] $L1_0$-FeNi is only found naturally in meteorites.[99] In 2015, Poirier *et al.* introduced tetragonal $L1_0$-FeNi obtained from the meteorite NWA 6259, presenting a large anisotropy field of 14.4 kOe (Fig. 7a).[41] Furthermore, in 2016 Lewis *et al.* reported tetragonal FeNi that was generated through an annealing protocol and pointed out the crystal structure transition of the FeNi lattice from a cubic to tetragonal unit cell, as shown in Fig. 7b.[100] Meanwhile, the chemical synthesis of $L1_0$-

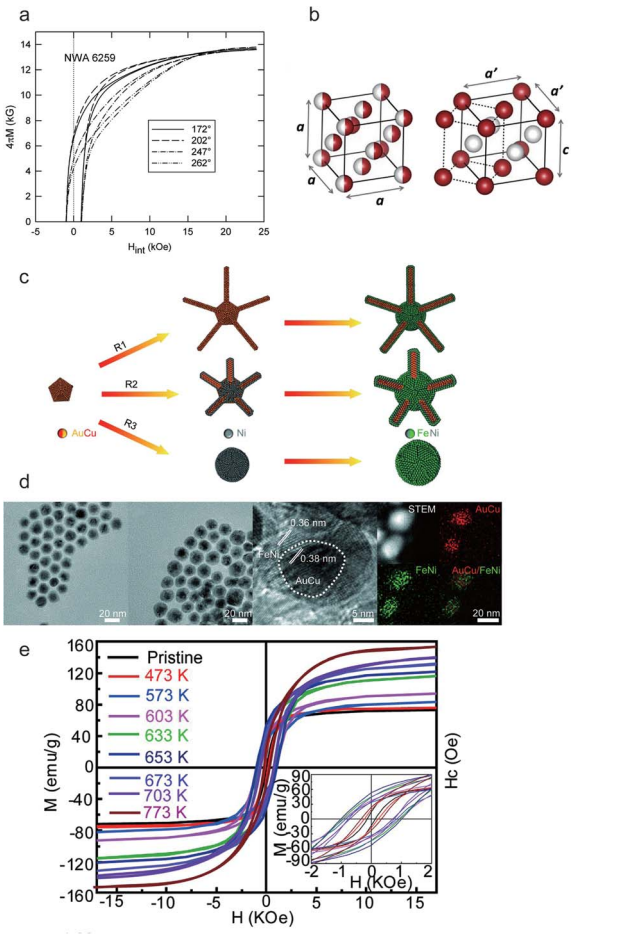

Fig. 7 (a) Magnetic hysteresis of NWA 6259 tetrataenite; (b) representations of the cubic (A1) and tetragonal ($L1_0$) unit cells of FeNi; (c) schematic images of the synthesis procedure of AuCu/FeNi (core/shell) nanocrystals; (d) TEM images of AuCu/FeNi (core/shell) nanostructures at different shell thicknesses. (e) The magnetic hysteresis loops of AuCu/FeNi (core/shell) nanocrystals with the stoichiometry of $Fe_{46}Ni_{54}$ at different annealing temperatures, and the inset images show the corresponding magnified hysteresis loops. Reproduced from ref. 84, 85 and 87 with the permission of AIP Publishing, Elsevier, and American Chemical Society.

FeNi was also presented by Hayashi *et al.* in 2013. The $L1_0$-FeNi alloy, prepared by a reductive reaction, showed a maximum coercivity of 220 kA m^{-1} (2765 Oe).[101] However, the stabilization of tetragonal FeNi alloys is a challenging task. In order to overcome this challenge, Ren introduced a rational epitaxial core/shell design to stabilize tetragonal FeNi nanocrystals (Fig. 7c). The reconstruction of tetragonal FeNi was triggered by the surface stress due to the existence of AuCu cores, as shown in Fig. 7d. The designed FeNi exhibited a large coercivity of 1010.2 Oe and a saturation magnetization of 122 emu g^{-1}, as shown in Fig. 7e.[102]

2.6 Fe_3Se_4

Fe_3Se_4, presenting a NiAs-type structure, has been studied due to its hard magnetic properties.[103] In 1956, Hirakawa suggested that the crystal of Fe_3Se_4 can be magnetized in the *c*-plane which is similar to Fe_7Se_8.[104] The ferrimagnetism of Fe_3Se_4 was generated by aligned spins within the *c*-plane.[105] Bishwas reported in 2014 a large increase in the energy product of Fe_3Se_4 up to 0.12 MGOe, as shown in Fig. 8a.[103] The synthesis of Fe_3Se_4 nanostructures doped with manganese has been proved to be a potential strategy to improve magnetic properties, such as the energy product. In 2011, Zhang *et al.* synthesized Fe_3Se_4 by organic-solution-phase chemical decomposition and showed that its high coercivity is 40 kOe at 10 K (Fig. 8b and c).[106,107] Among rare-earth-free magnets, Fe_3Se_4-based magnets are of intense interest. However, more advanced strategies aiming to improve Fe_3Se_4 are still urgent.[108]

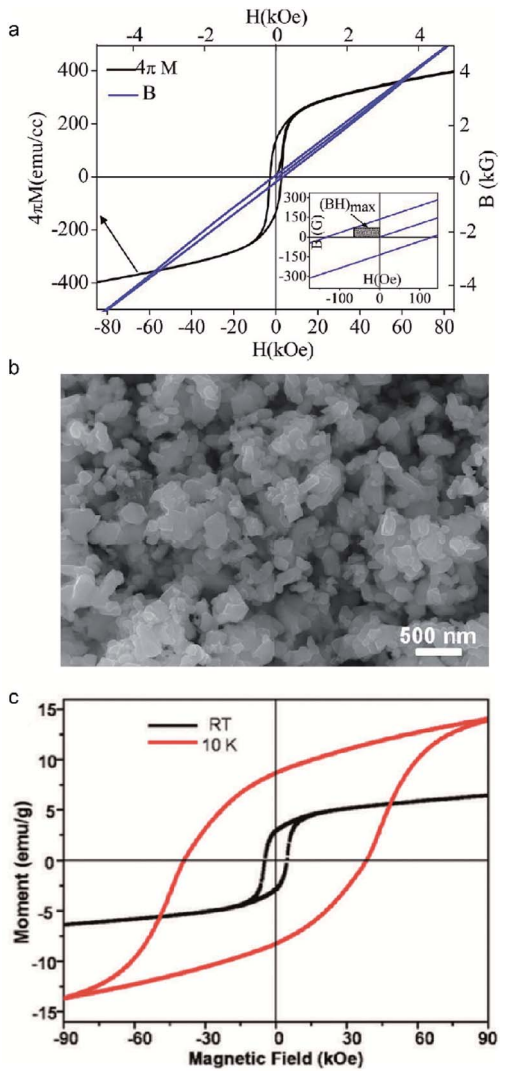

Fig. 8 (a) Magnetic characteristics of Fe_3Se_4 nanocrystals at 300 K. (Inset) Calculation of the maximum energy product of Fe_3Se_4; (b) typical SEM images of the as-synthesized Fe_3Se_4 nanoplatelets; (c) magnetic loops of faceted Fe_3Se_4 nanoparticles measured with a field of 90 kOe at 10 K and room temperature. Reproduced from ref. 88, 91 and 92 with the permission of American Chemical Society.

3 Conclusions

An overview of the existing and advanced manufacturing routes, developed in the past few decades, was explored and reviewed for rare-earth-free iron-based permanent magnets. The utility of versatile properties of iron-based magnets, such as coercivity and energy product, promotes the development of several permanent magnet candidates such as FePd, FePt, FeCo, $Fe_{16}N_2$, ε-Fe_2O_3, FeNi and Fe_3Se_4. Among the prepared FeCo phase, the optimal estimated energy product and coercivity achieved are 66 MGOe and 188 kOe. For FePd alloys, the maximum coercivity of 2.6 kOe and saturation magnetization of 190 emu g^{-1} showed the advantages of exchange-coupling. Meanwhile, the eutectic crystallization method indicated an advanced route to minimize the manufacturing procedure. The FePt magnet showed an optimal coercivity of 7.6 kOe with an optimum energy product of 5.0 MGOe. The $Fe_{16}N_2$ magnet presented a high coercivity of 1910 Oe and energy product of 20 MGOe. The coercivity of ε-Fe_2O_3 prepared in a silica template can be tunable from 31 kOe to 45 kOe. The rare-earth-free magnets, synthesized using iron-based precursors, play an important role in developing permanent magnets. The basic magnetic properties, such as coercivity and energy product, have been widely developed in several iron-based magnetic materials due to iron's low cost and abundance nature. However, the limitation of low energy product of rare-earth-free Fe-based magnets still poses a significant challenge for its practical applications, while the tunable magnetic properties achieved by doping could be a promising strategy to further improve their energy product. Therefore, the trend of permanent magnet development would focus on high magnetic performance in the foreseeable future accompanied by the extension of materials list.

Conflicts of interest

There are no conflicts to declare.

Acknowledgements

S. R. acknowledges the support from the U.S. National Science Foundation (NSF) under the CAREER Award No. NSF-DMR-1830749.

Notes and references

1 S. J. Galioto, P. B. Reddy, A. M. El-Refaie and J. P. Alexander, *IEEE Trans. Ind. Appl.*, 2014, **51**, 2148–2160.
2 M. Ghidini, R. Pellicelli, J. Prieto, X. Moya, J. Soussi, J. Briscoe, S. Dunn and N. Mathur, *Nat. Commun.*, 2013, **4**, 1–7.
3 S. Morimoto, Y. Tong, Y. Takeda and T. Hirasa, *IEEE Trans. Ind. Electron.*, 1994, **41**, 511–517.
4 M. Haavisto and M. Paju, *IEEE Trans. Magn.*, 2009, **45**, 5277–5280.
5 L. Chen, J. Wang, P. Lazari and X. Chen, Optimizations of a permanent magnet machine targeting different driving cycles for electric vehicles, *2013 International Electric Machines & Drives*, IEEE, 2013, pp. 855–862.
6 C. Stoeckert, Wind turbine driven generator to recharge batteries in electric vehicles, *US Pat.*, US3876925A, 1975.
7 L. Zhu and J. Zhao, *Appl. Phys. A: Mater. Sci. Process.*, 2013, **111**, 379–387.
8 J. Coey, *J. Magn. Magn. Mater.*, 2002, **248**, 441–456.
9 H. Kirchmayr, *J. Phys. D: Appl. Phys.*, 1996, **29**, 2763.
10 D. McDonald, *IEEE Trans. Magn.*, 1986, **22**, 1075–1077.
11 H. Nakamura, *Scr. Mater.*, 2018, **154**, 273–276.
12 K. Skokov and O. Gutfleisch, *Scr. Mater.*, 2018, **154**, 289–294.
13 M. H. Ghandehari, Rare earth-iron-boron-permanent magnets, *US Pat.*, US4952252A, 1990.
14 E. W. Blackmore, *IEEE Trans. Nucl. Sci.*, 1985, **32**, 3669–3671.
15 D. Lee, S. Bauser, A. Higgins, C. Chen, S. Liu, M. Huang, Y. Peng and D. Laughlin, *J. Appl. Phys.*, 2006, **99**, 08B516.
16 J. Cui, M. Kramer, L. Zhou, F. Liu, A. Gabay, G. Hadjipanayis, B. Balasubramanian and D. Sellmyer, *Acta Mater.*, 2018, **158**, 118–137.
17 E. Alonso, A. M. Sherman, T. J. Wallington, M. P. Everson, F. R. Field, R. Roth and R. E. Kirchain, *Environ. Sci. Technol.*, 2012, **46**, 3406–3414.
18 L. H. Lewis and F. Jiménez-Villacorta, *Metall. Mater. Trans. A*, 2013, **44**, 2–20.
19 Y. Jiang, M. Al Mehedi, E. Fu, Y. Wang, L. F. Allard and J.-P. Wang, *Sci. Rep.*, 2016, **6**, 25436.
20 M. Averbuch-Pouchot, R. Chevalier, J. Deportes, B. Kebe and R. Lemaire, *J. Magn. Magn. Mater.*, 1987, **68**, 190–196.
21 Y. Sun, J. Zhao, Z. Liu, W. Xia, S. Zhu, D. Lee and A. Yan, *J. Magn. Magn. Mater.*, 2015, **379**, 58–62.
22 N. Kleinerman, V. Serikov, N. Vlasova and A. Popov, *Philos. Mag.*, 2018, **98**, 2380–2396.
23 S. Okamoto, T. Shinozaki, T. Yamashita, N. Kikuchi and O. Kitakami, *J. Magn. Soc. Jpn.*, 2009, **33**, 451–454.
24 J. Liu, G. Guo, X. Zhang, F. Zhang, B. Ma and J.-P. Wang, *Acta Mater.*, 2020, **184**, 143–150.
25 M. Mohapatra and S. Anand, *Int. J. Eng. Sci. Technol.*, 2010, **2**, 127–146.
26 A. Figuerola, R. Di Corato, L. Manna and T. Pellegrino, *Pharmacol. Res.*, 2010, **62**, 126–143.
27 V. Brabers, *Phys. Status Solidi B*, 1969, **33**, 563–572.
28 R. Skomski, in *Novel Functional Magnetic Materials*, Springer, 2016, pp. 359–395.
29 C. Bean and D. Rodbell, *Phys. Rev.*, 1962, **126**, 104.
30 D. S. Mathew and R.-S. Juang, *Chem. Eng. J.*, 2007, **129**, 51–65.
31 D. Bahadur, S. Rajakumar and A. Kumar, *J. Chem. Sci.*, 2006, **118**, 15–21.
32 M. A. Willard, Y. Nakamura, D. E. Laughlin and M. E. McHenry, *J. Am. Ceram. Soc.*, 1999, **82**, 3342–3346.
33 R. Boll and H. Warlimont, *IEEE Trans. Magn.*, 1981, **17**, 3053–3058.
34 L. M. Rossi, N. J. Costa, F. P. Silva and R. Wojcieszak, *Green Chem.*, 2014, **16**, 2906–2933.
35 K. Maaz, A. Mumtaz, S. Hasanain and A. Ceylan, *J. Magn. Magn. Mater.*, 2007, **308**, 289–295.
36 X. Zhao, C.-Z. Wang, Y. Yao and K.-M. Ho, *Phys. Rev. B*, 2016, **94**, 224424.
37 S. Okamoto, O. Kitakami and Y. Shimada, *J. Appl. Phys.*, 1996, **79**, 5250–5252.
38 S. Ren and J. Yang, *Magnetic Nanomaterials: Fundamentals, Synthesis and Applications*, 2017.
39 G. Vashisht, R. Goyal, M. Bala, S. Ojha and S. Annapoorni, *IEEE Trans. Magn.*, 2018, **55**, 1–5.
40 N. H. Goo, Formation of hard magnetic L10-FePt/FePd monolayers from elemental multilayers, PhD thesis, University of Stuttgart, 2007.
41 E. Poirier, F. E. Pinkerton, R. Kubic, R. K. Mishra, N. Bordeaux, A. Mubarok, L. H. Lewis, J. I. Goldstein, R. Skomski and K. Barmak, *J. Appl. Phys.*, 2015, **117**, 17E318.
42 N. Vlasova, A. Popov, N. Kleinerman, V. Serikov, V. Gaviko and L. Stashkova, *Philos. Mag.*, 2019, **99**, 2198–2219.
43 A. A. El Gendy, J. M. Barandiaran and R. L. Hadimani, *Magnetic Nanostructured Materials From Lab to Fab*, Elsevier, 2018.
44 Y. Jin, W. Zhang, P. R. Kharel, S. R. Valloppilly, R. Skomski and D. J. Sellmyer, *AIP Adv.*, 2016, **6**, 056002.
45 C. Chinnasamy, M. M. Jasinski, A. Ulmer, W. Li, G. Hadjipanayis and J. Liu, *IEEE Trans. Magn.*, 2012, **48**, 3641–3643.
46 X. Guo, Z. Altounian and J. Ström-Olsen, *J. Appl. Phys.*, 1991, **69**, 6067–6069.
47 P. Manchanda, P. Kumar, A. Kashyap, M. Lucis, J. E. Shield, A. Mubarok, J. Goldstein, S. Constantinides, K. Barmak and L. Lewis, *IEEE Trans. Magn.*, 2013, **49**, 5194–5198.
48 H. Fang, S. Kontos, J. Ångström, J. Cedervall, P. Svedlindh, K. Gunnarsson and M. Sahlberg, *J. Solid State Chem.*, 2016, **237**, 300–306.
49 L. Zhou, M. K. Miller, P. Lu, L. Ke, R. Skomski, H. Dillon, Q. Xing, A. Palasyuk, M. McCartney and D. Smith, *Acta Mater.*, 2014, **74**, 224–233.
50 R. Skomski and D. Sellmyer, *J. Rare Earths*, 2009, **27**, 675–679.
51 S. Tumanski, *Organ*, 2010, **4**, 10.
52 A. López-Ortega, M. Estrader, G. Salazar-Alvarez, A. G. Roca and J. Nogués, *Phys. Rep.*, 2015, **553**, 1–32.
53 J. Coey, *IEEE Trans. Magn.*, 2011, **47**, 4671–4681.

54 J. M. Coey, *Magnetism and Magnetic Materials*, Cambridge university press, 2010.
55 J. Kim, Y. Lee and S. Sun, *J. Am. Chem. Soc.*, 2010, **132**, 4996–4997.
56 T. Osaka, M. Takai, K. Hayashi, K. Ohashi, M. Saito and K. Yamada, *Nature*, 1998, **392**, 796–798.
57 D. Wu, Q. Zhang, J. P. Liu, D. Yuan and R. Wu, *Appl. Phys. Lett.*, 2008, **92**, 052503.
58 A. Winkelmann, M. Przybylski, F. Luo, Y. Shi and J. Barthel, *Phys. Rev. Lett.*, 2006, **96**, 257205.
59 P. Warnicke, G. Andersson, M. Björck, J. Ferré and P. Nordblad, *J. Phys.: Condens. Matter*, 2007, **19**, 226218.
60 D. Kim and J. Hong, *Surf. Sci.*, 2012, **606**, 1960–1964.
61 G. Giannopoulos, L. Reichel, A. Markou, I. Panagiotopoulos, V. Psycharis, C. Damm, S. Fähler, I. Khan, J. Hong and D. Niarchos, *J. Appl. Phys.*, 2015, **117**, 223909.
62 I. Khan and J. Hong, *J. Phys. D: Appl. Phys.*, 2014, **47**, 415002.
63 M. Gong, A. Kirkeminde, M. Wuttig and S. Ren, *Nano Lett.*, 2014, **14**, 6493–6498.
64 L. Wu, A. Mendoza-Garcia, Q. Li and S. Sun, *Chem. Rev.*, 2016, **116**, 10473–10512.
65 K. Tanaka, T. Ichitsubo and M. Koiwa, *Mater. Sci. Eng., A*, 2001, **312**, 118–127.
66 A. Kirkeminde and S. Ren, *Nano Lett.*, 2014, **14**, 4493–4498.
67 J. Liu, in *Nanoscale Magnetic Materials and Applications*, Springer, 2009, pp. 309–335.
68 M. Chen and D. E. Nikles, *J. Appl. Phys.*, 2002, **91**, 8477–8479.
69 K. Sato and Y. Hirotsu, *Mater. Trans.*, 2006, **47**, 59–62.
70 K. Sato, B. Bian and Y. Hirotsu, *Jpn. J. Appl. Phys.*, 2000, **39**, L1121.
71 K. Watanabe, H. Kura and T. Sato, *Sci. Technol. Adv. Mater.*, 2006, **7**, 145.
72 Y. Hou, H. Kondoh, T. Kogure and T. Ohta, *Chem. Mater.*, 2004, **16**, 5149–5152.
73 Y. Yu, K. Sun, Y. Tian, X.-Z. Li, M. J. Kramer, D. J. Sellmyer, J. E. Shield and S. Sun, *Nano Lett.*, 2013, **13**, 4975–4979.
74 Z. Shao, L. An, Z. Li, Y. Huang, Y. Hu and S. Ren, *Chem. Commun.*, 2020, 6555–6558.
75 M. J. Bonder, Y. Huang and G. C. Hadjipanayis, in *Advanced Magnetic Nanostructures*, Springer, 2006, pp. 183–206.
76 L. Graf and A. Kussmann, *Z. Phys.*, 1935, **36**, 544–551.
77 B. Jeyadevan, K. Urakawa, A. Hobo, N. Chinnasamy, K. Shinoda, K. Tohji, D. D. J. Djayaprawira, M. Tsunoda and M. Takahashi, *Jpn. J. Appl. Phys.*, 2003, **42**, L350.
78 S. Sun, C. B. Murray, D. Weller, L. Folks and A. Moser, *science*, 2000, **287**, 1989–1992.
79 S. Sun, S. Anders, T. Thomson, J. Baglin, M. F. Toney, H. F. Hamann, C. Murray and B. D. Terris, *J. Phys. Chem. B*, 2003, **107**, 5419–5425.
80 M. Chen, J. Liu and S. Sun, *J. Am. Chem. Soc.*, 2004, **126**, 8394–8395.
81 J. Zhang, C. Li, J. Armstrong and S. Ren, *Chem. Commun.*, 2019, **55**, 656–658.
82 T. Ogawa, Y. Ogata, R. Gallage, N. Kobayashi, N. Hayashi, Y. Kusano, S. Yamamoto, K. Kohara, M. Doi and M. Takano, *Appl. Phys. Express*, 2013, **6**, 073007.
83 K. Jack, *J. Alloys Compd.*, 1995, **222**, 160–166.
84 T. Kim and M. Takahashi, *Appl. Phys. Lett.*, 1972, **20**, 492–494.
85 X. Bao, R. M. Metzger and M. Carbucicchio, *J. Appl. Phys.*, 1994, **75**, 5870–5872.
86 Y. Jiang, J. Liu, P. K. Suri, G. Kennedy, N. N. Thadhani, D. J. Flannigan and J. P. Wang, *Adv. Eng. Mater.*, 2016, **18**, 1009–1016.
87 A. Sivkov, E. Naiden, A. Ivashutenko and I. Shanenkov, *J. Magn. Magn. Mater.*, 2016, **405**, 158–168.
88 J. Sans, V. Monteseguro, G. Garbarino, M. Gich, V. Cerantola, V. Cuartero, M. Monte, T. Irifune, A. Muñoz and C. Popescu, *Nat. Commun.*, 2018, **9**, 1–11.
89 B. Wang, J. S. Chen, H. B. Wu, Z. Wang and X. W. Lou, *J. Am. Chem. Soc.*, 2011, **133**, 17146–17148.
90 J. Jin, S. i. Ohkoshi and K. Hashimoto, *Adv. Mater.*, 2004, **16**, 48–51.
91 S. Sakurai, K. Tomita, K. Hashimoto, H. Yashiro and S.-i. Ohkoshi, *J. Phys. Chem. C*, 2008, **112**, 20212–20216.
92 A. Namai, M. Yoshikiyo, K. Yamada, S. Sakurai, T. Goto, T. Yoshida, T. Miyazaki, M. Nakajima, T. Suemoto and H. Tokoro, *Nat. Commun.*, 2012, **3**, 1–6.
93 J. Kohout, P. Brázda, K. Závěta, D. Kubániová, T. Kmječ, L. Kubíčková, M. Klementová, E. Šantavá and A. Lančok, *J. Appl. Phys.*, 2015, **117**, 17D505.
94 S.-i. Ohkoshi, K. Imoto, A. Namai, S. Anan, M. Yoshikiyo and H. Tokoro, *J. Am. Chem. Soc.*, 2017, **139**, 13268–13271.
95 M. Kotsugi, C. Mitsumata, H. Maruyama, T. Wakita, T. Taniuchi, K. Ono, M. Suzuki, N. Kawamura, N. Ishimatsu and M. Oshima, *Appl. Phys. Express*, 2009, **3**, 013001.
96 J. Pauleve, D. Dautreppe, J. Laugier and L. Néel, *J. Phys. Radium*, 1962, **23**, 841–843.
97 K. Reuter, D. B. Williams and J. Goldstein, *Metall. Trans. A*, 1989, **20**, 711–718.
98 T. Kojima, M. Mizuguchi, T. Koganezawa, K. Osaka, M. Kotsugi and K. Takanashi, *Jpn. J. Appl. Phys.*, 2011, **51**, 010204.
99 J. Mohapatra and J. P. Liu, in *Handbook of Magnetic Materials*, Elsevier, 2018, vol. 27, pp. 1–57.
100 A. Montes-Arango, L. Marshall, A. D. Fortes, N. Bordeaux, S. Langridge, K. Barmak and L. Lewis, *Acta Mater.*, 2016, **116**, 263–269.
101 Y. Hayashi, S. Gotou, M. Mizuguchi, M. Kotsugi, Y. Kitou, E. Okuno and K. Takanashi, *J. Magn. Soc. Jpn.*, 2013, **37**, 198–201.
102 M. Gong and S. Ren, *Chem. Mater.*, 2015, **27**, 7795–7800.
103 M. Sen Bishwas, R. Das and P. Poddar, *J. Phys. Chem. C*, 2014, **118**, 4016–4022.
104 K. Hirakawa, *J. Phys. Soc. Jpn.*, 1957, **12**, 929–938.
105 D. Li, D. Pan, S. Li and Z. Zhang, *Sci. China: Phys., Mech. Astron.*, 2016, **59**, 617501.
106 H. Zhang, G. Long, D. Li, R. Sabirianov and H. Zeng, *Chem. Mater.*, 2011, **23**, 3769–3774.
107 G. Long, H. Zhang, D. Li, R. Sabirianov, Z. Zhang and H. Zeng, *Appl. Phys. Lett.*, 2011, **99**, 202103.
108 D. Li, Y. Li, D. Pan, Z. Zhang and C.-J. Choi, *J. Magn. Magn. Mater.*, 2019, **469**, 535–544.